ChemCatChem

Research Article
doi.org/10.1002/cctc.202300673

Chemistry Europe
European Chemical Societies Publishing

www.chemcatchem.org

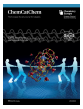

First-principles Assessment of the Role of Water in the Reduction Half Cycle of Low-Temperature NH_3-SCR over Cu-CHA

Gabriele Contaldo,[a] Matteo Ferri,[a] Chiara Negri,[a] Isabella Nova,[a] Matteo Maestri,[a] and Enrico Tronconi*[a]

Dispersion corrected density functional theory calculations show that the presence of H_2O in the Reduction Half-Cycle (RHC) of NH_3-SCR affects the free energy of the kinetically-relevant transition state (TS) leading to a reduction in the rate and activation energy with respect to dry conditions. In particular, H_2O enthalpically stabilizes the kinetically-relevant TS by 20 kJ mol^{-1} with respect to the dry counterpart. Such enthalpic stabilization vanishes when van der Waals (vdW) interactions are excluded from the calculations, thus showing the preeminent role of non-specific dispersion forces in the reduction of the activation enthalpy. At the same time, the enthalpic stabilization is more than compensated by the additional entropy losses of the TS brought forth by the presence of H_2O in the CHA cage. Calculated enthalpy and entropy changes with respect to the dry case agree quantitatively with the experimental measurements and reflect the modified reacting environment in the presence of H_2O. As a result, this study provides theoretical underpinnings on the mechanistic role of H_2O in the RHC and, on a more general basis, highlights the importance of the molecular scale description of the reaction environment in voids of molecular dimensions.

Introduction

Copper-exchanged chabazite (CHA) zeolites are the state-of-the-art catalysts for the abatement of NO_x emissions from vehicles exhausts via selective catalytic reduction (SCR) of NO by NH_3.[1–4] These materials show excellent performances in catalyzing the Low-Temperature (LT) Standard SCR, a process that has attracted extensive research interest for the emission control in sustainable mobility. Recent studies have shown that the Standard SCR reaction (R.1) can be described by a redox chemistry,[5,6] which consists in a Reduction Half-Cycle (RHC), where Cu active sites change their oxidation state from Cu^{II} to Cu^{I}, and in the subsequent re-oxidation step (OHC).

$$4NH_3 + 4NO + O_2 \rightarrow 4N_2 + 6H_2O \quad \text{(R.1)}$$

The structure of Cu intermediates involved in the reaction pathway are nonetheless still debated in the literature.[7–9] As a matter of fact, single and binuclear Cu moieties have been proposed as the active sites for both OHC and RHC. Focusing on the RHC, the main argument in favor of a single-site Cu^{II} reduction mechanism relies on a weak dependence of apparent first-order rate constants on the Cu density.[5,10,11] Recent studies based on transient kinetic analysis and CO titration experiments combined with electronic structure calculations and consistent with *in situ/operando* spectroscopy seem to confirm however that the RHC follows a binuclear Cu^{II}-pathway.[12–16] In fact, a dual-site mechanism was proposed by Hu et al.[12] for the reduction of Cu^{II} active sites, studying the reducibility of the oxidized active sites in dry conditions, i.e., according to an experimental protocol that excludes H_2O from the reactor feed stream. In particular, two individual co-caged $Cu^{II}(OH)(NH_3)_3$ moieties, identified as two-proximate (Two-P), are involved in the NO oxidative activation to HONO, documented as the relevant kinetic step of the RHC. This molecular structure, suggested as a plausible unstable intermediate during RHC in dry conditions,[6] reacts with one NH_3 ligand to form NH_4NO_2 that finally decomposes to N_2 and H_2O. The same reaction steps are then involved in the reduction of the second Cu^{II} active site. This reaction pathway is consistent with the experimental observations,[15] which reveal that the overall LT-RHC proceeds at a rate proportional to NO pressures and with a quadratic dependency on Cu^{II}.

Gramigni et al. further studied this reacting system in the presence of H_2O in the reacting feed,[17] a technologically relevant aspect to consider in this redox chemistry because abundantly present in real SCR conditions. The work indicates that the addition of H_2O to the reactor feed stream does not

[a] G. Contaldo, Dr. M. Ferri, Dr. C. Negri, Prof. I. Nova, Prof. M. Maestri, Prof. E. Tronconi
Laboratory of Catalysis and Catalytic Processes
Dipartimento di Energia
Politecnico di Milano
Via la Masa 34
20156 Milano (Italy)
E-mail: matteo.maestri@polimi.it
enrico.tronconi@polimi.it

Supporting information for this article is available on the WWW under https://doi.org/10.1002/cctc.202300673

affect the binuclear nature of Cu^{II} moieties and reports that the RHC in wet conditions still proceeds with second order kinetics in Cu^{II}. Moreover, the presence of H_2O in the feed stream approximately halves the apparent activation energy of the RHC in dry conditions, while on the contrary reduces the reaction rate inhibiting the RHC.

There is not a general consensus regarding the mechanistic reasons for such an effect. Thus, theoretical underpinnings are required to clarify the kinetic role of H_2O in this reacting environment at the molecular scale. To this aim, here we employ dispersive corrected density functional theory (DFT) calculations[18–20] to examine the role of H_2O in the RHC of the NH_3-assisted SCR.

We first study the interactions between H_2O with NO species and the Two-P complex in the cage of CHA according to free energy calculations. This analysis shows that the contact of NO and H_2O gives rise to strong enthalpic stabilization effects that favor the selected configuration in terms of free energy of adsorption. According to this result, we then identify the final state (FS) structure in the presence of H_2O, in order to examine the pathway of the kinetically-relevant step of NO activation to HONO under wet conditions and thus make a comparison with the dry case. We show that wet conditions influence the Gibbs free energy of the kinetically-relevant transition state (TS) structure due to confinement, which reflects enthalpic stabilization and concomitant entropic penalties. In particular, we find that the presence of H_2O in the cage of Cu-CHA produces stronger enthalpic stabilization effects compared to the dry conditions, thus leading to a reduction of the apparent activation enthalpy. At the same time, the presence of H_2O induces a penalty in terms of entropy losses at the examined temperatures of the RHC ($<$ 493 K), due to the reduced mobility of the TS in the cage. These entropic losses more than compensate for the enthalpic stabilization, thus decreasing the RHC rate as compared to the dry case. These findings are fully in line with the relevant role of the reacting environment at the atomic scale in affecting the rate of the reaction.[21,22] Moreover, such investigations establish a mechanistic analogy between the dry and wet reaction pathways and elucidate the detailed chemistry that regulates the RHC of the NH_3-SCR reaction under wet conditions.

Methods

Density functional theory (DFT) calculations were performed using the planewaves-pseudopotential approach as implemented in the QuantumEspresso package.[23] We employed optimized norm-conserving Vanderbilt pseudopotential[24] to model the electron-ion interaction and we set a kinetic energy cutoff of 80 Ry (~1088 eV) to converge the total energy per atom within 0.01 eV. The Brillouin zone sampling was restricted to the Γ-point. We adopted the hybrid Heyd-Scuseria-Ernzerhof (HSE06) exchange and correlation functional[25] for better estimates of reaction energies involving NO species, as pointed out by Paolucci et al.[10,26] All the calculations were performed including spin polarization effects and the Grimme-D_3 correction[27] is accounted for long-range van der Waals dispersion forces. The crystal structure of the Cu-CHA was modeled using a rhombohedral 12-T site unit cell, with a Si : Al ratio equal to 10 : 2 and 36 atoms, $a = b = c$ =0.94 nm and $\alpha = \beta = \gamma$ =94.6°. The Al atoms in the cage were placed at third-nearest-neighbor (3NN) position in the 6 MR structure, which represents the energetically favored site according to previous calculations.[10] All the atoms in the zeolite framework were kept fixed, while the suspended molecules (Two-P as the binuclear Cu^{II} active site, NO in the initial state configuration, HONO as the product of the reaction and H_2O) were allowed to relax into the cage of Cu-CHA. The convergence criterion for the forces on each atom was set to 0.001 eV Å^{-1}. The change in the oxidation state of Cu during the reduction step is investigated by means of the Bader charge analysis[28] by comparing the charges assigned to Cu atoms with those computed for bulk Cu_2O and CuO, taken as reference for Cu(I) and Cu(II), respectively. To reduce the computational cost, the mobile structures were first relaxed using the Perdew, Burke and Ernzerhof (PBE)[29] exchange and correlation functional and subsequently optimized using HSE06.[21,30] The transition state (TS) geometry of the kinetically-relevant step under wet and dry conditions were identified using the Climbing-Image Nudged Elastic Band (CI-NEB) method using a convergence threshold on the forces of 0.05 eV Å^{-1}. We performed the vibrational analysis using the finite-difference approximation of the Hessian matrix as implemented in Atomic Simulation Environment (ASE).[31] For gas phase molecules, a relaxation calculation was performed in a cubic cell with $a = b = c$ =1.5 nm.

Statistical thermodynamics methodologies were adopted to describe the entropy, enthalpy and Gibbs free energy for the species involved in the dry and wet reactions in order to include temperature dependency (the computational details are reported in the Supporting Information, Section I). All the gas phase species were assumed ideal and the contributions of translations, rotations and vibrations were modeled with the ideal gas approximation as implemented in ASE. Confined species were treated following two distinct approaches. The TS structure, which consists in the complex formed between NO and OH, is modeled with the harmonic limit approximation because all the motions of the structure relative to the zeolite are found to be frustrated. Therefore, the overall entropy is calculated by treating all the 3 N degrees of freedom of the complex harmonically, because the translational and rotational contribution are zero. On the other hand, NO, HONO and H_2O in the cage are mobilized and retain part of their translational and rotational degrees of freedom.[32–34] Therefore, we scaled by a factor of 2/3 their gas-phase translational and rotational contributions for a reasonable evaluation of the total entropy in the confined environment, following the methodology proposed by Chen et al.[14] Only the vibrations of OH attached to Two-P are included in the calculations because it is the only ligand in the active site complex that takes part in the NO oxidative activation to HONO.

Results and Discussion

The experimental evidence reported by Gramigni et al. shows that, in the presence of H_2O in the feed stream, the RHC exhibits the same rate dependencies of the dry conditions mechanism as proposed by Hu et al., and consistent with recent experimental investigations.[12,15,17] In line with these interpretations, the reaction proceeds at a rate proportional to the NO partial pressure and with a quadratic dependency on Cu^{II}. This reaction mechanism identifies the NO activation to HONO as the relevant kinetic step that regulates the overall RHC.[12] Such analogies in the kinetic mechanisms thus suggest that the reaction in wet conditions is characterized by the same kineti-

cally- relevant step (i.e., the elementary step that exhibits the highest free energy along the reaction coordinate). For this reason, the effects of wet conditions on the RHC of NH_3-SCR are here explored by studying the kinetically-relevant step of reduction introducing one H_2O molecule in the cage of CHA. The inclusion of two H_2O molecules is assessed in the Supporting Information, Section II. In particular, experiments show that the presence of H_2O affects the apparent rate constant of the reaction by decreasing the observed apparent activation enthalpy from 55 to 30 kJ mol^{-1}, while on the contrary inhibiting the RHC by decreasing the reaction rate.

Given the similarity in the kinetic mechanisms, we describe the apparent activation enthalpy and entropy in analogy with the dry counterpart by including the presence of one H_2O in the calculations. For consistency with the experimental measurements, we adopt as a common reference state for both the reactions in dry and wet conditions the energy of isolated reactants in gas phase, that is NO and H_2O, and the uncharged Cu-CHA, which accounts for the presence of co-caged Cu^{II}-moieties in the form of Two-P.[12] Thus, we define the apparent activation enthalpy and entropy of the reaction in the presence of H_2O as expressed in Eq. 1 and Eq. 2:

$$\Delta H^{\ddagger}_{app} = H^{\ddagger}_{KRS,conf} - H_{NO,gas} - H_{H_2O,gas} - H_{ZCuOH(NH_3)_3} \quad (1)$$

$$\Delta S^{\ddagger}_{app} = S^{\ddagger}_{KRS,conf} - S_{NO,gas} - S_{H_2O,gas} - S_{ZCuOH(NH_3)_3} \quad (2)$$

$H^{\ddagger}_{KRS,conf}$ and $S^{\ddagger}_{KRS,conf}$ are the enthalpy and the entropy of the kinetically-relevant TS structure in the presence of H_2O in the zeolite. $H_{NO,gas}$, $H_{H_2O,gas}$ and $S_{NO,gas}$, $S_{H_2O,gas}$ refer to the enthalpy and entropy of the relevant gas phase reactants, while $H_{ZCuOH(NH_3)_3}$ and $S_{ZCuOH(NH_3)_3}$ correspond to the uncharged zeolite in the presence of co-caged Cu^{II}-moieties as active sites, which define the reference for our calculations. Hence, in order to provide a mechanistic explanation to such an effect, we compute the change in the observed apparent activation enthalpy and entropy in the presence of H_2O with respect to the dry counterpart.

The interactions between Two-P, NO and H_2O give rise to several local minima along the potential energy surface (PES) which correspond to different geometries,[35] as a consequence of the formation of mobile complexes suspended in the zeolite cage at low-temperature conditions.[36] In this specific case, the two moieties of Cu^{II} solvated by NH_3 occupy a large volume in the cage, hence the relative position of the guest molecule of H_2O is influenced by the presence of steric interactions with the mobile sites, limiting its free mobility within the cavity. Therefore, we study the position of H_2O with respect to the Two-P structure and NO upon confinement with the aim to understand the relative stability of the initial state (IS) geometry in terms of free energy of adsorption.

We here report in Figure 1 the three configurations A, B and C, which show the contribution of one H_2O molecule in the cage of Cu-CHA. Further considerations on the addition of two H_2O molecules are reported in Section II of the Supporting Information.

Configurations A and B show H_2O being placed in the regions above the upper moiety and below the lower moiety of Two-P, according to the reference system adopted in the figure. On the other hand, structure C represents the only configuration in which H_2O resides in the region of the cavity that allows for concomitant interactions with both Cu^{II} species. According to our analysis, these structures represent the only accessible minimum energy configurations because, after any possible translation and rotation, the molecule always falls in the same local minima. Moreover, in all the cases H_2O does not affect the planar tetra-coordinated structure of Cu^{II}, confirming the less affinity for ligating with Cu compared to NH_3.[10] These results demonstrate the presence of different local minima along the PES and reflect the different interactions of mobile species with the environment.

We observe that the H_2O molecule in configuration C is relaxed at a distance from the closest Cu^{II} moiety equal to 2.4 Å, which is comparable to the same quantity evaluated for structures A and B, respectively equal to 2.3 Å and 2.7 Å. On the contrary, the relative position of H_2O with respect to NO is strongly influenced by the steric limitations induced by Two-P. Configuration C shows NO located adjacent to H_2O and oriented towards the OH group anchored to Two-P at a distance equal to 2.7 Å. Instead, the contact between H_2O and NO is significantly reduced by the presence of the steric limitations caused by the presence of Two-P, which lead to increase the distance up to 5 Å and 5.1 Å in configuration A and B, respectively.

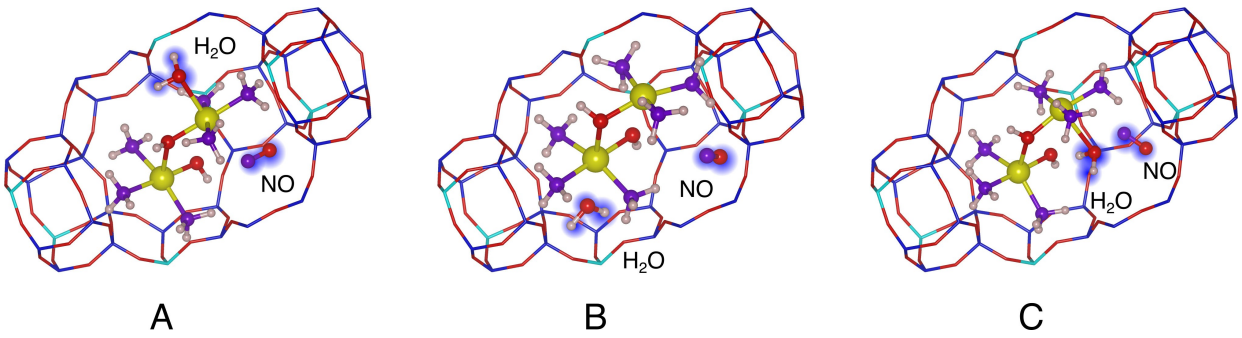

Figure 1. Configurations for the initial state (IS) structure under wet conditions confined in the cage of Cu-CHA. Structure A corresponds to the H_2O molecule relaxed above the upper moiety of Two-P. Structure B coincides with H_2O located below the lower moiety of Two-P. Structure C refers to the configuration obtained with H_2O interacting with both Cu^{II} sites. List of atoms: Blue = Si, Red = O, Yellow = Cu, Green = Al, Violet = N, Grey = H.

We account for temperature dependency by calculating the adsorption enthalpy, entropy and free energy of the IS configuration under wet conditions. The DFT-derived thermodynamic parameters are reported in Table 1 at a temperature of 150 °C and 1 bar. It is evident the strong exothermic adsorption of −84 kJ mol^{-1} calculated for configuration C, while significantly lower values are observed for A and B, equal to −46 kJ mol^{-1} and −50 kJ mol^{-1}, respectively. The reasons of such different stabilization effects are elucidated performing a Bader charge analysis on the H_2O molecule added in the different IS configurations. We observe no differences in the charges assigned to the oxygen atom in H_2O (−2e) in all the three systems, as compared to the same quantity calculated in the gas phase molecule, taken as reference. Hence, the larger enthalpic stabilization observed for configuration C is a sole consequence of stronger electronic stability resulting from the proximity between NO and H_2O, which leads to a more negative value of its total energy with respect to the other considered cases. Thus, we observe no charge transfer between H_2O and NO upon confinement. As a result, these differences in the adsorption enthalpies show that a closer proximity of H_2O to NO lead to larger enthalpic stabilization upon confinement.

On the other hand, the reduction of the reaction volume up to molecular dimensions produce concomitant entropic penalties which disfavor the confined structures in terms of free energy.[21,37] These effects are stronger than in dry conditions due to the presence of H_2O which further reduces the limited available space in Cu-CHA, thus resulting in larger losses of translational and rotational entropy. The visualization and detailed analysis of all the frequencies associated to the H_2O species upon confinement indicate the presence of 2D free translations and rotations, because mobilized molecules in voids of molecular dimensions retain part of their translational and rotational degrees of freedom from gas phase.[32–34] Thus, we scale by a factor of 2/3 the gas-phase translational and rotational contributions (details in the Supporting Information, Section I), as proposed by Chen et al.[14] The same approach adopted for the NO molecule once again reflects the presence of 2D roto-translations in the vibrational frequencies in the range of 0 to 100 cm^{-1}.

Table 1 shows that the entropic contributions are almost constant in all the cases (from −90 to −97 J mol^{-1} K^{-1}), because of the similar zero-point vibrational energy calculated in the three geometries. The slight difference of 7 J mol^{-1} K^{-1} is explained in terms of the reduced distance of NO and H_2O relaxed in configuration C, which favors the stabilization in terms of enthalpy at the cost of more hindered mobility. Accordingly, such entropic losses strongly reduce the beneficial enthalpic stabilization for configuration A and B, leading to an adsorption free-energy of −8 kJ mol^{-1} and −10 kJ mol^{-1}. Instead, the larger enthalpic effects observed for configuration C prevails over these entropic penalties and lead to a more negative free-energy of adsorption of −43 kJ mol^{-1}, as shown in Table 1. Such evidence highlight that H_2O is preferentially located in the region of the cage which exhibits stronger interactions with NO, thus leading to an overall decrease of the distance between the species. As a result, configuration C is the most stable one in terms of free energy and we adopted it for the evaluation of the transition state structure of the RHC reaction under wet conditions, in order to make a comparison with the dry case.

Following the identification of the IS in the wet case (Figure 2(a)), we examine the FS geometry accounting for the relative interactions between HONO and H_2O. The optimized structure is reported in Figure 2(c), which reflects the reduction of Cu^{II} into Cu^{I} because of the loss of one OH group from the upper moiety of Two-P. We observe a change in the oxidation state of Cu^{II} with respect to the IS geometry when applying a Bader charge analysis.[28] More precisely, we compare the charges assigned to Cu atoms in the oxidized (+1.01e) and reduced (+0.60e) sites with those computed for the bulk CuO (+0.93e) and in Cu_2O (+0.53e) phases, taken as representative of the Cu^{II} and Cu^{I} species, respectively.[38,39] The result shows a clear difference in the Bader-computed oxidation states of the active site in wet conditions, which reproduces the effective

Table 1. DFT-derived enthalpies, entropies and Gibbs free energies of adsorption with respect to the gas-phase reference state (NO, H_2O and empty Cu-CHA) at 150 °C and 1 bar for configurations A, B and C in Figure 1.

Configurations	$H_{IS}-H_{ref}$ [kJ mol^{-1}]	$S_{IS}-S_{ref}$ [J mol^{-1} K^{-1}]	$G_{IS}-G_{ref}$ [kJ mol^{-1}]
A	−46	−90	−8
B	−50	−94	−10
C	−84	−97	−43

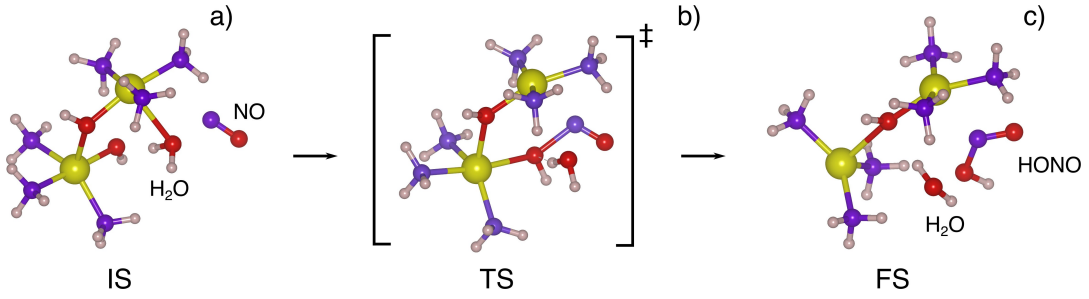

Figure 2. Initial state (IS), final state (FS) and transition state (TS) for the kinetically-relevant step of NO oxidative activation to HONO in the presence of H_2O in the cage of Cu-CHA. The framework of CHA is avoided for a better visualization of molecular structures. List of atoms: Red = O, Yellow = Cu, Violet = N, Grey = H.

reduction of Cu^{II} into Cu^{I} during the NO activation step. Moreover, a direct comparison between the Cu charges observed in the wet system with the oxidized (1.07 e) and reduced (+0.57 e) Cu charges evaluated for the dry mechanism shows that the presence of H_2O does not alter the oxidation state of Cu during the reduction, thus ruling out any charge transfer with Two-P.

The TS of the kinetically-relevant step of the RHC under wet conditions (Figure 2(b)) is finally investigated with the Climbing Image Nudge Elastic Band (CI-NEB) methodology in the presence of H_2O in the proximity of Two-P and NO. In analogy to the dry mechanism, the OH group is detached from the Two-P moiety and a bond is created with the approaching NO species, with a length of 1.67 Å. We verify the presence of one single imaginary frequency along the reaction coordinate by evaluating the vibrational energies for the transition state structure (NO + OH) and the adjacent H_2O molecule (as reported in the Supporting Information, Section III). The analysis reveals that the vibrational modes of the TS and H_2O are not correlated because the vibrational spectrum is unaffected when the two species are treated simultaneously or independently, thus showing that H_2O is not directly involved in the reaction mechanism. Instead, the presence of H_2O strongly influences the energy of the TS structure by means of dispersive forces, which are favored by the reduced distance with (NO + OH). As a result, H_2O presence favors the stabilization of the TS structure upon confinement, leading to a reduction of the apparent activation energy with respect to the dry counterpart of 20 kJ mol^{-1}.

We now relate these electronic energies at 0 K to Gibbs free energies to allow a comparison with the experimental measurements in the range of temperature from 150 °C to 220 °C. Figure 3 shows the enthalpy (a), entropy (b) and Gibbs free energy

(c) diagrams relative to each state of the kinetically-relevant step either in wet and dry conditions. As reported in Figure 3(a), the reaction enthalpy associated to the wet mechanism (blue line) is endothermic by 15 kJ mol^{-1}, in agreement with the slight endothermicity computed for the dry system of 3 kJ mol^{-1} (black line). Moreover, the enthalpic barrier of the NO activation step in the presence of H_2O is equal to 126 kJ mol^{-1}, which is notably larger than the corresponding value computed in dry conditions (80 kJ mol^{-1}). However, the confinement conferred by the presence of H_2O in the proximity of the TS structure induces a net decrease of the apparent barrier as compared to the dry case. Figure 3(a) highlights that the apparent activation enthalpy in wet conditions is reduced by 20 kJ mol^{-1} with respect to the dry counterpart equal to 42 kJ mol^{-1}, in contrast with 62 kJ mol^{-1} computed for the dry case. This result is in good agreement with the experimentally observed apparent barrier of 30 kJ mol^{-1} reported by Gramigni et al.[17] and confirms the behavior of the net decrease of the apparent activation energy under wet conditions in terms of the enthalpic stabilization of the TS structure. It is worth mentioning that such stabilization completely vanishes when van der Waals forces are excluded from the calculations. In fact, we observe that the difference in the apparent activation enthalpy

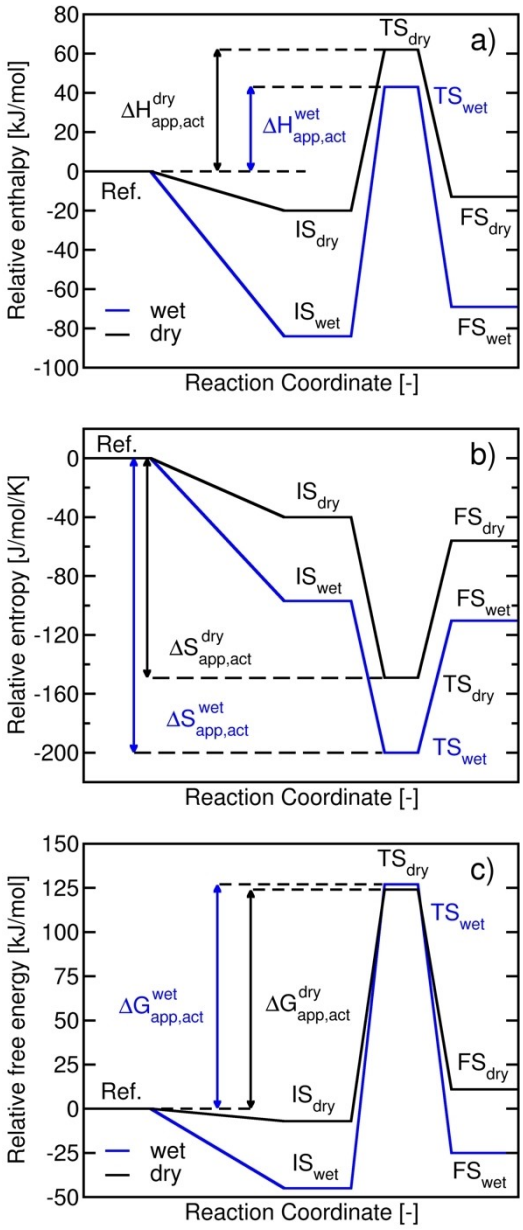

Figure 3. Relative enthalpy (a), relative entropy (b) and relative Gibbs free energy (c) for the kinetically-relevant step of RHC under wet (blue path) and dry (black path) conditions. Ref. = NO_{gas}, H_2O_{gas} and empty CHA. IS = NO confined in the cage of CHA under wet and dry conditions. FS = HONO confined in the cage of CHA under wet and dry conditions.

between the wet and dry mechanisms decreases to 4 kJ mol^{-1} (Supporting Information, section IV), thus showing that H_2O stabilization effects are strongly dominated by van der Walls contributions.

At the same time, the effects of void dimensions in the presence of H_2O induce large entropy losses upon confinement that disfavor the enthalpic stabilization of the TS. We computed the entropic contribution for the transition state structure (NO + OH) and H_2O with two different approaches (Supporting Information, Section I). The motions associated to the TS are modelled within the harmonic oscillator (HO) approximation, corroborated by a detailed analysis and visualization of normal

modes associated to frequencies in the range of 0 to 100 cm^{-1}, which reveal that all motions relative to the zeolite are frustrated. On the other hand, the entropy associated to the H_2O molecule is computed by scaling the translational and rotational gas-phase entropy by a factor of 2/3, in analogy with the discussion reported for the initial state. The same model is applied for the FS structure because the hydroxyl group is completely detached from the Cu^{II} active site, therefore the intermediate HONO is free to move in the cage because its vibrations are not completely frustrated. We verify that the total entropic penalties associated to the TS under wet conditions are significantly larger than the same quantity computed for the dry system. As shown in Figure 3(b), the apparent activation entropy is the lowest value along the path, almost equal to $-200\ J\,mol^{-1}\,K^{-1}$, as compared to the dry case ($-150\ J\,mol^{-1}\,K^{-1}$). This finding is the consequence of the translational and rotational contributions that H_2O retains upon confinement from gas phase, thus leading to additional entropic penalties with respect to the dry case. Our estimates are in line with the measurements that reveal an entropic penalty of $-160\ J\,mol^{-1}\,K^{-1}$ for the dry system and $-220\ J\,mol^{-1}\,K^{-1}$ in wet conditions. Such investigation is in good analogy with the experimental trend observed by Gramigni et al.[17] because we are able to predict the inhibition effects of the RHC under wet conditions on the basis of larger entropic losses, after the addition of H_2O in the cage of CHA. These H_2O effects are appreciated in the calculation of the Gibbs free energy, as reported in Figure 3(c). The diagram shows how wet conditions slightly increase the apparent activation free energy with respect to the dry system (from 125 $kJ\,mol^{-1}$ to 127 $kJ\,mol^{-1}$), making entropies a strong contribution in affecting the activation free energies. As a result, the rate of the RHC is reduced due to entropic limitations, even with an observed and computed decrease of the apparent activation enthalpy. Therefore, the observed H_2O effects on the RHC only reflects the changes in the enthalpy and entropy of the kinetically-relevant TS, which directly affect the observed rates for the dry and wet mechanisms.

The rate constants for the wet and dry systems are calculated according to the harmonic transition state theory (TST) and compared to the experimental observations in Figure 4(a). The straight dashed lines represent the simulations, whose slopes denote the apparent activation enthalpy equal to 42 and 62 $kJ\,mol^{-1}$ in the case of wet and dry conditions, respectively. The symbols show the experimental estimates collected over 1.7% Cu-CHA.[17] The trend observed in the diagram shows a decrease of the rate constants in both cases for the low temperature range (right part in Figure 4(a)). The good agreement between measured and DFT-derived rates further suggests that the transition state structure of the NO activation under wet conditions represents the real kinetically-relevant structure of the entire reduction step. It is worth noting that, either in the wet or dry case, the theoretical apparent activation enthalpies (62 $kJ\,mol^{-1}$ in dry and 42 $kJ\,mol^{-1}$ for the wet system, respectively) overestimate by around 10 $kJ\,mol^{-1}$ the corresponding measurements (55 $kJ\,mol^{-1}$ and 30 $kJ\,mol^{-1}$). These outcomes lead to a slight underestimation of the experimental data at low temperatures, as shown in the right part of Figure 4(a). Such a deviation is possibly related to the difference between the theoretical SAR of 10 adopted in the calculations, consistent with the 2Al crystal structure of Cu-CHA, and the actual SAR of 25 in the tested sample.[17] The Al density is known to affect the overall standard NH_3-SCR rates,[40,41] therefore such a difference may have caused the slight variation observed in Figure 4(a). Notably, such a difference in SAR between theory and experiments is present both in wet and dry conditions. Thus, following the procedure proposed by Maestri and Iglesia,[21] to directly isolate the effect of H_2O and get rid of the SAR effects, here we report in Eq. 3 the results in terms of the ratio between the wet and dry reaction rates:

$$\zeta = \frac{r_{wet}}{r_{dry}} = exp\left(\frac{\Delta S^{\ddagger}}{R}\right) exp\left(-\frac{\Delta H^{\ddagger}}{RT}\right) \quad (3)$$

where $\Delta H^{\ddagger}$ and $\Delta S^{\ddagger}$ correspond to the difference between the apparent activation enthalpy and entropy for the wet and dry reactions. Figure 4(b) shows the ratio between the wet and dry

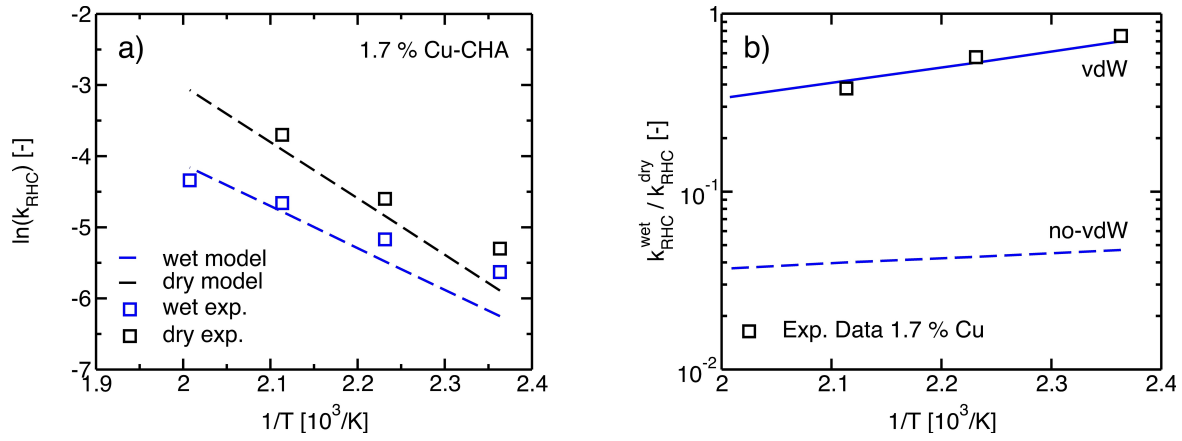

Figure 4. a) DFT-derived Arrhenius plots of the 2nd order reduction rate constants (k_{app}) under wet and dry conditions compared to experimental data at 1.7% of Cu-CHA, as reported by Gramigni et al.[16] b) Ratio between the wet and dry rate constants compared to the experimental data in[16] calculated by including and excluding dispersive forces.

Table 2. Rate constants, apparent activation enthalpies, entropies and Gibbs free energies (200 °C and 1 bar) for the kinetically-relevant step of RHC under wet and dry conditions. K^{DFT}_{RHC} = DFT-derived rate constant. k^{exp}_{RHC} = measured rate constant.[16]

Reaction	k^{DFT}_{RHC} [10^{-3} s^{-1}]	k^{exp}_{RHC} [10^{-3} s^{-1}]	$\Delta H_{app,act}$ [kJ mol^{-1}]	$\Delta S_{app,act}$ [J mol^{-1} K^{-1}]	$\Delta G_{app,act}$ [kJ mol^{-1}]
Dry	20	25	62	−150	125
Wet	8.4	9.5	42	−200	127

apparent rate constants, represented by the blue curve, compared to the experimental observations, square points. The agreement between experiments and calculations is excellent. In particular, the ratio approaches the unity at low temperature while instead decreases at higher temperature. This result indicates that H_2O effects are more evident at high T due to the stronger entropic penalties contribution in this range. Therefore, entropic losses lead to smaller observed RHC rates under wet conditions, a phenomenon which is especially noteworthy at high temperature. The exclusion of the van der Waals contributions from the calculations lead to a drastic decrease of the ratio (Eq. 3), as reported with the dashed blue line in Figure 4(b). As a result, the stabilization effects of H_2O on the catalytic cycle become irrelevant because the entropic losses completely dominate over the negligible enthalpic stabilization calculated excluding the van der Waals dispersion contributions, in analogy with the catalysis by confinement description of catalyzed reactions in voids of molecular dimensions.[21,42] A direct comparison between the dry and wet thermodynamic parameters and the theoretical and measured rate constants is reported in Table 2 at 200 °C and 1 bar.

The results show that the theoretical reaction rates accurately reproduce the experiments in the range of temperature analyzed, as a consequence of the modified reacting environment in the presence of H_2O. Therefore, we conclude that the experimentally observed H_2O effects on the RHC are a consequence of a trade-off between enthalpic stabilization and entropic penalties. In particular, the enthalpic contribution reduces the observed activation energy of the kinetically-relevant step, while the additional entropic penalties brought forth by H_2O in the cage of Cu-CHA disfavor the free movement of the TS structure in the cavity and strongly inhibit the reaction rate. Measured rates only reflect the difference of entropy and enthalpy of the kinetically-relevant TS under wet and dry conditions, thus accounting for the catalysis by confinement as a fundamental role in the detailed mechanistic description of NH_3-assisted SCR in Cu-CHA at molecular level.

Conclusions

The detailed description of the reaction path under wet conditions led us to establish a direct comparison between the dry and wet RHC mechanisms at a molecular level. We provide by means of dispersive-corrected density functional theory (DFT) calculations the theoretical description of the effects of H_2O in the RHC of the NH_3-assisted SCR over Cu-CHA. In particular, we observe a decrease of 20 kJ mol^{-1} in the apparent activation enthalpy of the RHC under wet conditions (42 kJ mol^{-1}) with respect to the dry counterpart (62 kJ mol^{-1}), as a consequence of the enthalpic stabilization of the TS in the presence of H_2O. At the same time, the entropic penalties in the wet system are sufficiently large to reduce the beneficial effects of stabilization with respect to the dry case, thus resulting in larger entropic losses upon confinement (from −150 J mol^{-1} K^{-1} to −200 J mol^{-1} K^{-1}). Such entropic penalties resulting by the addition of H_2O in the cage of Cu-CHA more than compensate for the enthalpic stabilization of the TS, thus leading to a reduction of the reaction rate of the RHC. The excellent agreement with experimental data reported by Gramigni et al.[17] is observed when comparing the ratio between the wet and dry reaction rates, which only reflects the change of the TS enthalpy and entropy between the wet and dry systems as a consequence of the modified reacting environment in the presence of H_2O. Such enthalpic stabilization effects completely vanish when the van der Waals forces are excluded from the calculations, thus making entropy the prevalent contribution in the rate of the RHC. This observation is in analogy with the catalysis by confinement effects, thus proving its fundamental role in the RHC of NH_3-assisted SCR in Cu-CHA under realistic wet conditions and thus highlighting the importance of the molecular scale description of the reaction environment in voids of molecular dimensions.

Supporting Information

Additional computational methods are reported in the Supporting Information. Electronic Structure Calculations, statistical thermodynamics methodologies, calculation of the reaction rate, geometries, including vibrational frequencies and coordinates, related to all the structures studied, CI-NEB calculations excluding vdW interactions, contribution of two H_2O in the model.

Acknowledgements

Computational time at CINECA, Bologna (Italy) is gratefully acknowledged under the ISCRA projects for the availability of high-performance computing resources. The calculations were performed on Galileo100 under the project REDCAT (ISCRA C).

Conflict of Interests

The authors declare no conflict of interest.

Data Availability Statement

The data that support the findings of this study are available in the supplementary material of this article.

Keywords: NH_3-SCR · Reduction-Half-cycle · H_2O effects · reaction mechanism · DFT

[1] I. Nova, E. Tronconi, *Urea-SCR Technology for DeNOx after Treatment of Diesel Exhausts*, Springer, **2014**.
[2] C. K. Lambert, *React. Chem. Eng.* **2019**, *4*, 969–974.
[3] A. Wang, L. Olsson, *Nat. Catal.* **2019**, *2*, 566–570.
[4] E. Borfecchia, P. Beato, S. Svelle, U. Olsbye, C. Lamberti, S. Bordiga, *Chem. Soc. Rev.* **2018**, *47*, 8097–8133.
[5] T. V. W. Janssens, H. Falsig, L. F. Lundegaard, P. N. R. Vennestrøm, S. B. Rasmussen, P. G. Moses, F. Giordanino, E. Borfecchia, K. A. Lomachenko, C. Lamberti, others, *ACS Catal.* **2015**, *5*, 2832–2845.
[6] F. Gao, D. Mei, Y. Wang, J. Szanyi, C. H. F. Peden, *J. Am. Chem. Soc.* **2017**, *139*, 4935–4942.
[7] K. A. Lomachenko, E. Borfecchia, C. Negri, G. Berlier, C. Lamberti, P. Beato, H. Falsig, S. Bordiga, *J. Am. Chem. Soc.* **2016**, *138*, 12025–12028.
[8] C. Paolucci, I. Khurana, A. A. Parekh, S. Li, A. J. Shih, H. Li, J. R. Di Iorio, J. D. Albarracin-Caballero, A. Yezerets, J. T. Miller, W. N. Delgass, F. H. Ribeiro, W. F. Schneider, R. Gounder, *Science* **2017**, *357*, 898–903.
[9] F. Gao, E. D. Walter, M. Kollar, Y. Wang, J. Szanyi, C. H. F. Peden, *J. Catal.* **2014**, *319*, 1–14.
[10] C. Paolucci, A. A. Parekh, I. Khurana, J. R. Di Iorio, H. Li, J. D. Albarracin Caballero, A. J. Shih, T. Anggara, W. Nicholas Delgass, J. T. Miller, F. H. Ribeiro, R. Gounder, W. F. Schneider, *J. Am. Chem. Soc.* **2016**, *138*, 6028–6048.
[11] C. B. Jones, I. Khurana, S. H. Krishna, A. J. Shih, W. N. Delgass, J. T. Miller, F. H. Ribeiro, W. F. Schneider, R. Gounder, *J. Catal.* **2020**, *389*, 140–149.
[12] W. Hu, T. Selleri, F. Gramigni, E. Fenes, K. R. Rout, S. Liu, I. Nova, D. Chen, X. Gao, E. Tronconi, *Angew. Chem. Int. Ed.* **2021**, *60*, 7197–7204.
[13] A. Martini, C. Negri, L. Bugarin, G. Deplano, R. K. Abasabadi, K. A. Lomachenko, T. V. W. Janssens, S. Bordiga, G. Berlier, E. Borfecchia, *J. Phys. Chem. Lett.* **2022**, *13*, 6164–6170.
[14] L. Chen, T. V. W. Janssens, P. N. R. Vennestrøm, J. Jansson, M. Skoglundh, H. Gronbeck, *ACS Catal.* **2020**, *10*, 5646–5656.
[15] D. J. Deka, R. Daya, A. Ladshaw, S. Y. Joshi, W. P. Partridge, *Chem. Eng. J.* **2022**, *435*, 134219.
[16] R. Villamaina, U. Iacobone, I. Nova, M. P. Ruggeri, J. Collier, D. Thompsett, E. Tronconi, *ChemCatChem* **2020**, *12*, 3843–3848.
[17] F. Gramigni, N. D. Nasello, N. Usberti, U. Iacobone, T. Selleri, W. Hu, S. Liu, X. Gao, I. Nova, E. Tronconi, *ACS Catal.* **2021**, *11*, 4821–4831.
[18] P. Nachtigall, J. Sauer, *Stud. Surf. Sci. Catal.* **2007**, 701–736.
[19] J. Hafner, L. Benco, T. Bučko, *Top. Catal.* **2006**, *37*, 41–54.
[20] F. Göltl, A. Grüneis, T. Bučko, J. Hafner, *J. Chem. Phys.* **2012**, *137*, 114111.
[21] M. Maestri, E. Iglesia, *Phys. Chem. Chem. Phys.* **2018**, *20*, 15725–15735.
[22] M. Maestri, *Chem. Commun.* **2017**, *53*, 10244–10254.
[23] P. Giannozzi, S. Baroni, N. Bonini, M. Calandra, R. Car, C. Cavazzoni, D. Ceresoli, G. L. Chiarotti, M. Cococcioni, I. Dabo, A. D. Corso, S. de Gironcoli, S. Fabris, G. Fratesi, R. Gebauer, U. Gerstmann, C. Gougoussis, A. Kokalj, M. Lazzeri, L. Martin-Samos, N. Marzari, F. Mauri, R. Mazzarello, S. Paolini, A. Pasquarello, L. Paulatto, C. Sbraccia, S. Scandolo, G. Sclauzero, A. P. Seitsonen, A. Smogunov, P. Umari, R. M. Wentzcovitch, *J. Phys. Condens. Matter* **2009**, *21*, 395502.
[24] D. R. Hamann, *Phys. Rev. B* **2013**, *88*, 85117.
[25] J. Heyd, G. E. Scuseria, *J. Chem. Phys.* **2004**, *121*, 1187–1192.
[26] C. Paolucci, A. A. Verma, S. A. Bates, V. F. Kispersky, J. T. Miller, R. Gounder, W. N. Delgass, F. H. Ribeiro, W. F. Schneider, *Angew. Chem. Int. Ed.* **2014**, *53*, 11828–11833.
[27] E. Caldeweyher, C. Bannwarth, S. Grimme, *J. Chem. Phys.* **2017**, *147*, 34112.
[28] G. Henkelman, A. Arnaldsson, H. Jónsson, *Comput. Mater. Sci.* **2006**, *36*, 354–360.
[29] J. P. Perdew, K. Burke, M. Ernzerhof, *Phys. Rev. Lett.* **1996**, *77*, 3865.
[30] W.-G. Liu, W. A. Goddard III, *J. Am. Chem. Soc.* **2012**, *134*, 12970–12978.
[31] A. H. Larsen, J. J. Mortensen, J. Blomqvist, I. E. Castelli, R. Christensen, Marcin Dułak, J. Friis, M. N. Groves, B. Hammer, C. Hargus, E. D. Hermes, P. C. Jennings, P. B. Jensen, J. Kermode, J. R. Kitchin, E. L. Kolsbjerg, J. Kubal, Kristen Kaasbjerg, S. Lysgaard, J. B. Maronsson, T. Maxson, T. Olsen, L. Pastewka, Andrew Peterson, C. Rostgaard, J. Schiøtz, O. Schütt, M. Strange, K. S. Thygesen, Tejs Vegge, L. Vilhelmsen, M. Walter, Z. Zeng, K. W. Jacobsen, *J. Phys. Condens. Matter* **2017**, *29*, 273002.
[32] B. A. De Moor, M.-F. Reyniers, G. B. Marin, *Phys. Chem. Chem. Phys.* **2009**, *11*, 2939–2958.
[33] R. Gounder, E. Iglesia, *Acc. Chem. Res.* **2012**, *45*, 229–238.
[34] M. Jørgensen, L. Chen, H. Grönbeck, *J. Phys. Chem. C* **2018**, *122*, 20351–20357.
[35] L. Chen, H. Falsig, T. V. W. Janssens, J. Jansson, M. Skoglundh, H. Grönbeck, *Catal. Sci. Technol.* **2018**, *8*, 2131–2136.
[36] F. Giordanino, E. Borfecchia, K. A. Lomachenko, A. Lazzarini, G. Agostini, E. Gallo, A. V. Soldatov, P. Beato, S. Bordiga, C. Lamberti, *J. Phys. Chem. Lett.* **2014**, *5*, 1552–1559.
[37] N. Artioli, R. F. Lobo, E. Iglesia, *J. Phys. Chem. C* **2013**, *117*, 20666–20674.
[38] Y. Wang, S. Lany, J. Ghanbaja, Y. Fagot-Revurat, Y. P. Chen, F. Soldera, D. Horwat, F. Mücklich, J. F. Pierson, *Phys. Rev. B* **2016**, *94*, 245418.
[39] L. Chen, T. V. W. Janssens, H. Grönbeck, *Phys. Chem. Chem. Phys.* **2019**, *21*, 10923–10930.
[40] F. Gao, N. M. Washton, Y. Wang, M. Kollár, J. Szanyi, C. H. F. Peden, *J. Catal.* **2015**, *331*, 25–38.
[41] S. H. Krishna, A. Goswami, Y. Wang, C. B. Jones, D. P. Dean, J. T. Miller, W. F. Schneider, R. Gounder, *Nat. Catal.* **2023**, 1–10.
[42] R. Gounder, E. Iglesia, *Chem. Commun.* **2013**, *49*, 3491–3509.

Manuscript received: June 27, 2023
Revised manuscript received: July 21, 2023
Accepted manuscript online: July 21, 2023
Version of record online: August 15, 2023